

CANDID: Correspondence Alignment for Deep-burst Image Denoising

Arijit Mallick*[§]

Department of Computer Graphics
University of Tübingen, Germany
arijit.mallick@uni-tuebingen.de

Raphael Braun

Department of Computer Graphics
University of Tübingen, Germany
raphael.braun@uni-tuebingen.de

Hendrik PA Lensch

Department of Computer Graphics
University of Tübingen, Germany
hendrik.lensch@uni-tuebingen.de

Abstract—With the advent of mobile phone photography and point-and-shoot cameras, deep-burst imaging is widely used for a number of photographic effects such as depth of field, super-resolution, motion deblurring, and image denoising. In this work, we propose to solve the problem of deep-burst image denoising by including an optical flow-based correspondence estimation module which aligns all the input burst images with respect to a reference frame. In order to deal with varying noise levels the individual burst images are pre-filtered with different settings. Exploiting the established correspondences one network block predicts a pixel-wise spatially-varying filter kernel to smooth each image in the original and prefiltered bursts before fusing all images to generate the final denoised output. The resulting pipeline achieves state-of-the-art results by combining all available information provided by the burst.

Keywords—Burst photography; Denoising; Image alignment;

I. INTRODUCTION

Due to recent development of faster and lightweight portable CPUs especially in mobile and point-and-shoot cameras, burst photography has been gaining further prominence because of the noise reduction and motion blur removal capabilities. Burst photography [1, 2] can also be understood as multi-frame image restoration task [3–6] which has a wider range of applications even in satellite photography [7, 8] for remote sensing. The sensors and lenses in smartphones are much smaller and more lightweight than those of professional cameras but they collect less light per pixel which leads to noisier images. Compensating this by longer exposures could introduce motion blur. As an alternative, a burst of many short and noisy images could be computationally combined into one sharp image. Camera phone APIs already provide denoising algorithms but they are not optimized for burst denoising.

Current burst denoising methods perform the alignment simply based on homographies estimated between the burst images [9, 10], followed by some pixel denoising. Our proposed pixel-wise alignment based on optical flow is significantly more powerful in compensating for scenes with complex depth and camera or object motion. We still expect the motion between the burst images to be rather small. Our overall architecture is depicted in Figure 1. First, we generate enhanced burst inputs by applying the pre-trained self-guided filtering network

(SGN) [11] for each image to generate pre-denoised bursts. Both, the original and the denoised images are aligned with respect to the reference frame using the RAFT [12] optical flow network. Based on the aligned images and extracted features a network block predicts a per-pixel adaptive filter kernel to denoise every pixel in every image. A final fusion block merges all predictions across all bursts into a single output.

Secondly, we estimate pixel adaptive filter-kernels which per pixel describe where to collect color information from the aligned input bursts. The decoder then only applies those kernels, thus produces weighted averages over neighbouring pixels from all aligned images.

We demonstrate the importance of each module in an ablation study. Our contributions are as follows: a) optical flow-based alignment of multiple pre-denoised burst images, b) adaptive per-pixel filtering of aligned burst images followed by cross-burst fusion, c) improved denoising performance, especially in low-noise scenarios.

II. RELATED WORK

Related work covers single image denoising, homography-based alignment, and deep-burst imaging. In the following section, we discuss related works pertaining to our problem statement, starting with single image denoising, followed by homography-based and optical flow-based alignment, and finally contemporary progress on deep-burst imaging.

a) *Single image denoising*: Most photography hardware companies take advantage of the recently developed lightweight neural network denoising models; exploiting the significant increase in mobile computation power. In the early days of CNNs, models such as [11] improved performance compared to classical image denoising models based on Markov random fields but they could not compete with BM3D [13] which introduced a new denoising paradigm by combining 3D block matching and domain transform. They are later surpassed by a sparse denoising autoencoder models [14, 15]. Simple multi-layer perceptron-based models [16], residual link networks [17] and later deeper residual networks [18] and persistent memory-based networks [19] have shown superior performance due to enhanced receptive fields. All these models have the advantage of being trainable end-to-end exploiting simple to generate training data. For a multitude of image processing

[§]This work was done while Mr. Arijit Mallick was affiliated with University of Tübingen, Germany. He is currently working for TWT GmbH Science & Innovation, Germany.

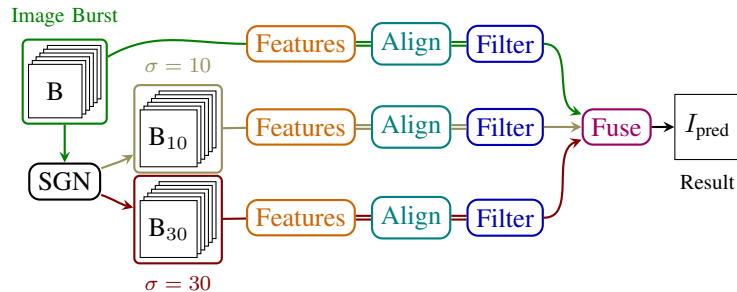


Figure 1. Method overview. The input **image burst** is pre-filtered twice using SGN [11] with different filter strengths. For each stack we extract **features**, **align** both features and images and then apply a content-adaptive spatial **filter** with weights derived from the aligned features. The results from all three bursts are **fused** to predict the denoised output.

tasks, training can be accelerated using pre-trained models and transfer learning [20]. In this spirit, we incorporate the pre-trained self-guided network (SGN) [11] to enrich the burst input with smooth priors. SGN extracts large-scale contextual information and gradually propagates it to the higher resolution sub-networks for feature self-guidance and denoising at multiple scales. This efficient multiscale local features extraction property allows it to efficiently recover denoised images.

b) Deep-burst Denoising: While single image denoising relies on learned image priors, deep-burst denoising assimilates features from multiple noisy frames to predict a better image. A similar idea is used in burst motion deblurring [21] where a sharp image is recurrently extracted from a burst of blurry ones. Similarly, recurrent neural networks have also been used for burst denoising. Bhat et al. [10] reparametrize the image formation process in the latent space, and integrate learned image priors for the denoised prediction. Kernel prediction networks [22, 23] leverage the localized pixel neighborhood weighted filters to predict a denoised image from multiple inputs. Dudhane et al. [24] proposed to extract pre-processed features from each burst frame following an edge-boosting burst alignment module. The pseudo-burst features are then enriched using multi-scale contextual information, which is followed by adaptively aggregate information from the corresponding features.

Our novel burst denoising model also applies adaptive pixel-neighborhood filters but first performs an explicit alignment step.

c) Correspondence Alignment: Multiple frame denoising usually involves some sort of alignment [5] of the frames in the burst for superior feature assimilation. Tico [25] demonstrates a block matching approach within the reference and the neighboring frames to support multiple frame denoising. VBM4D [26] and VBM3D [27] take the BM3D algorithm further to video denoising with faster homography flow-based alignment. We instead estimate per pixel correspondences for a more fine-grained alignment. When capturing a burst of images of a potentially dynamic scene with a handheld camera each image will show slightly different content. In order to effectively utilize information from those multiple frames for denoising, the frames need to be aligned [5].

Tico [25] demonstrates a block matching approach within the reference and the neighboring frames to support multiple frame denoising. VBM4D [26] and VBM3D [27] take the BM3D algorithm further to video denoising with block matching for alignment.

Neural network optical flow models can leverage information beyond patch-level correspondence information to predict dense correspondences, i.e. estimating pixel motion between consecutive frames of a video [28]. Some of the first learning based optical flow methods used simple CNN architectures [29–31]. Recently they were superseded by recurrent techniques like RAFT [12] or transformer-based architectures like FlowFormer [32]. Those current state of the art techniques are very good and very close to ground truth [33].

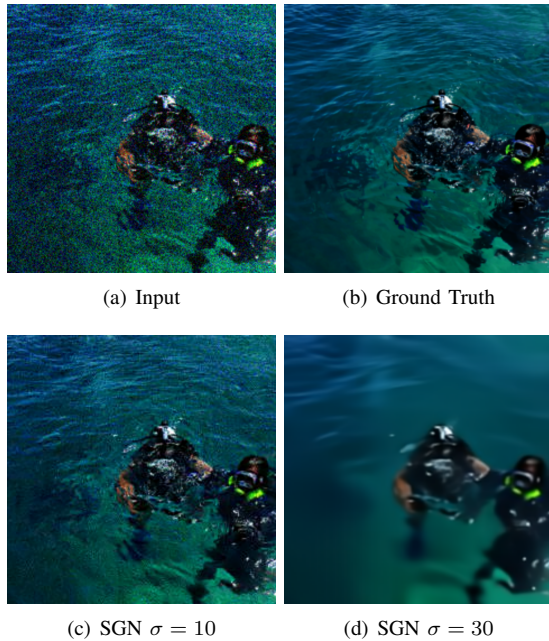
In our approach we utilize the success in the optical flow field by using a pretrained RAFT implementation provided in torchvision [34]. RAFT provides the high-quality pixel-wise correspondence alignment that we rely on for our denoising approach.

III. METHOD

The core idea of our burst denoising method is to first spatially align the pixels in the burst stack. Afterwards, each aligned image is denoised by a content-adaptive spatially-varying filter step followed by an adaptive fusion of all processed images (see Figure 1, left).

A. Prefiltering with SGN

Our method starts by filtering the burst images. The amount of noise in input bursts can vary significantly, even within the same burst. Because of varying degrees of noise and blur due to abrupt camera motion, precise alignment might be difficult. We, therefore, duplicate the input burst into three processing streams. The first stream B uses the original burst, the second stream B_{10} ($\sigma = 10$) a mildly pre-denoised version of the burst and the last one B_{30} ($\sigma = 30$) a strongly denoised version (see Figure 2). We apply the pretrained SGN [11] to each individual frame but any single-frame denoising algorithm could be used. The intermediate results from the different streams will be fused in the last step of our pipeline.



(c) SGN $\sigma = 10$ (d) SGN $\sigma = 30$
 Denoising performance of the pre-trained SGN. ($\sigma = 10$) retains the original sharpness. ($\sigma = 30$) shows better denoising performance but loses sharp details.

Figure 2. Prefiltering with SGN



(a) Reference (b) before alignment (c) after alignment
 Alignment error between the reference and the last burst image scaled 5 times. Note, how after alignment differences in the silhouette are no longer present.

Figure 3. Pixel-wise alignment

B. Feature Extraction

To add local context to each pixel we enrich each image by processing it with a simple CNN. In addition, the estimated noise level of the image is concatenated as the fourth channel before processing. In each processing stream, we produce corresponding feature stacks. The same shared weights are used for each image in each stream. Both the image stack and the feature stack are used as inputs for the alignment module.

C. Alignment

The central property that is exploited with burst denoising is that the content captured in the individual frames of the burst is very similar. In the original images, the scene content however might be shifting due to camera shake or scene dynamics. We use the pre-trained RAFT [12] model that is shipped with torchvision [34] to estimate the optical flow between

the reference image frame and any other image frame in the burst. The estimated flow computed from the reference and secondary images is used to warp the secondary image frames and their corresponding feature maps with respect to the reference image frame and the reference feature frame respectively. The effectiveness of the RAFT-based alignment is visualized in Figure 3.

D. Collaborative Content-adaptive Spatial Filtering

At this point, the images and features in the bursts are all aligned with respect to the reference frame. The next step is to filter the images spatially and combine the results pixel-wise for the final result. The spatial filtering is implemented with content-dependent per-pixel kernels. Those kernels are estimated by a CNN from the aligned feature stack, i.e. collaboratively considering all feature maps at the same time. The output activations of this CNN are reshaped into 3×3 and 5×5 filter kernels for all images and all pixels. The result is two kernels of shape $[N, H, W, 3, 3]$ and $[N, H, W, 5, 5]$ with the number of images N , height H and width W . The kernels are normalized via *softmax* and applied to each image in the burst individually, effectively computing a weighted average color over the 3×3 and 5×5 neighborhood of each pixel as shown in Figure 4.

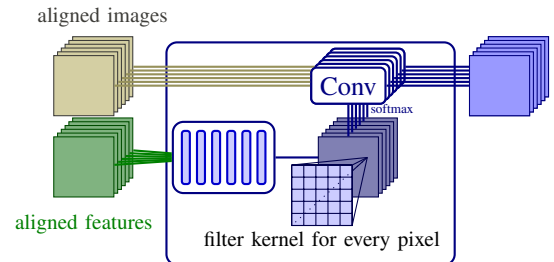


Figure 4. The spatial content-adaptive filter kernels for every pixel are estimated by a CNN based on all aligned features. They are applied individually to the aligned images to produce the spatially filtered burst.

E. Burst Fusion

Remember in Section III-A the burst was split into three processing streams B , B_{10} and B_{30} , which are all processed individually in the same way so far. This means at this stage we have aligned and spatially filtered images and the corresponding aligned image features for each stream. The final step is to fuse all information from the different bursts into a single denoised image I_{pred} . This denoised result is computed as a weighted average over the spatially filtered images from all three processing streams. As indicated in Figure 5, we concatenate the aligned features of the streams with the spatially filtered images and process them together in a 4-layer CNN. This CNN produces the weight volume. This volume contains a weight for every pixel and color of every image. A softmax over the image dimension is applied to the weights in order to ensure that summing up the weights over this dimension yields 1 for every color channel. The result I_{pred} is finally computed as a weighted sum per pixel. This is implemented as element-wise multiplication between weight volume and

spatially filtered images followed by a sum over the burst dimension. Every channel for every input image is therefore weighted individually, which is more powerful than just mixing the existing colors of the spatially filtered images.

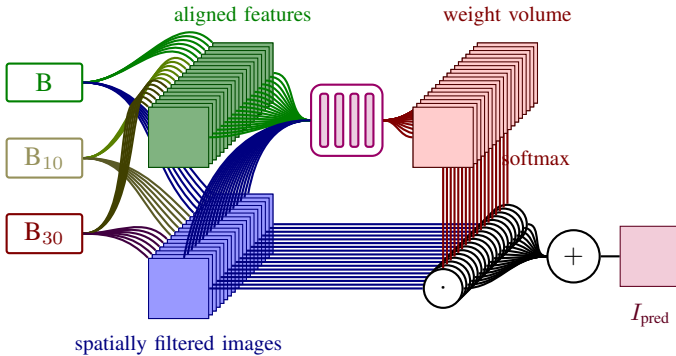


Figure 5. Fusion Network. The aligned features from all three bursts are concatenated with the spatially filtered images and processed by a CNN to obtain a weight volume. The weights are used to compute the denoised result as a weighted per-pixel sum over the spatially filtered images.

F. Training

Some components of the denoising pipeline like the SGN and the alignment module are pretrained. We stopped the gradients from going through the SGN networks, which effectively turns the three burst streams B, B₁₀ and B₃₀ into separate inputs. The RAFT network in the alignment module was frozen and used as fixed differentiable operation. The remaining trainable weights are in the CNNs for the feature extractor, the content-adaptive cooperative spatial filter, and the burst fusion module. We train end-to-end with ADAM [35] from a simple L1-loss $\mathcal{L} = \|I_{\text{pred}} - I_{\text{gt}}\|_1$ on the ground truth I_{gt} .

IV. EXPERIMENTS

We evaluate our method by comparing to state of the art and validate our architecture choices with an ablation study.

A. Training and experimental setup

For the pre-denoising we use the SGN pre-trained with $\sigma = 10, 30$ [36]. For the burst denoising training both the SGN pre-denoising and the RAFT alignment model are frozen. We trained on the OpenImages [37] dataset and evaluated on the grayscale burst benchmark [22] and RGB burst benchmark following the usual conventions [10, 23, 24]. The ground truth images are shifted and corrupted by adding heteroscedastic Gaussian noise [38] with variance $\sigma_r^2 + \sigma_s^2 x$. Here x is the clean pixel value, while σ_r and σ_s denote the readout and shot noise parameters, respectively. Those noise parameters are assumed to be known both during training and testing, and are used in the feature extractor. During training they are sampled uniformly in the log-domain from the range $\log(\sigma_r) \in [-3, -1.5]$ and $\log(\sigma_s) \in [-4, -2]$. The comparisons are evaluated with 2 different noise lvl.1 and lvl.2, corresponding to noise parameters (-2.2, -2.6) and (-1.8, -2.2) respectively. Training was done on 2 TITAN Xp GPUs and took about 96 hours to converge.

model	Color		Grayscale	
	lvl. 1	lvl. 2	lvl. 1	lvl. 2
KPN [22]	38.38	35.96	36.47	33.93
BPN [39]	40.16	37.08	38.18	35.42
MFIR-1 [10]	40.16	37.08	39.37	36.51
MFIR-2 [10]	42.21	39.13	39.37	36.51
BIPNET [24]	42.28	40.20	41.26	38.74
Ours	42.49	39.18	41.35	36.61

Table I

PSNR VALUES OF THE EVALUATION GRAYSCALE BURST DATASET. BLUE SHOWS BEST RESULTS WHILE GREEN SHOWS THE SECOND BEST RESULTS. lvl. INDICATES THE LEVEL OF GAUSSIAN NOISE ADDED ACCORDING TO EVALUATION CONVENTION.

B. Results

The quantitative comparison with other methods in Table IV-B shows that our model delivers overall state-of-the-art performance the aforementioned benchmark in the evaluation of the model-unseen dataset. On deep introspection, we can say that due to SGN and further multiple kernel-based filtering, the model successfully recovers the image even from the heavy noise scenarios. In the future, one could add additional SGN-based denoising stages with different pre-trained noises to analyze whether further boosting of lvl.1 and lvl.2 would be possible. Additionally, larger filter kernels can be added to the model in order to enhance the results for higher noise scenarios.

Exemplar qualitative results on individual images are shown in Figure 6

C. Ablation Study

Model	lvl.1 gray
without SGN pre-denoising	40.81
without RAFT alignment	38.54
without content-adaptive filtering	41.27
Ours – complete pipeline	41.35

Table II

ABLATION STUDY. REMOVING THE INDIVIDUAL PARTS OF THE PIPELINE AND TRAINING THE MODEL FROM SCRATCH REVEALS THE IMPORTANCE OF EACH COMPONENT. ONLY BY COMBINING SGN-BASED PRE-DENOSING, FLOW-BASED ALIGNMENT AND CONTENT-ADPATIVE FILTERING GOOD PERFORMANCE IN HIGHT NOISE LEVELS CAN BE ACHIEVED.

Since our module consists of several pretrained blocks and trainable sub-modules, we analyse the effectiveness of each of the components with the corresponding ablation in Table II. Here, we removed individual parts of the pipeline and trained the network from scratch. Removing all SGN blocks effectively suppresses pre-denoising of the input. Although the low-noise evaluation performs comparatively well, image quality deteriorates as the noise increases due to the lack of cleaner proposals at the initial stages. Without the alignment module, the final fusion step is impaired and we see lower performance on all noise levels. Particularly lvl.1 is impacted.

Finally, the cooperative content-adaptive filtering adds almost equally to the reconstruction quality of all noise levels levels.

D. Qualitative Results

In Figure 6 we demonstrate the improved performance of our pipeline on a number of example images. Even for drastically different amount of noise our approach outperforms BIPNET [24] on every image. The denoised image is significantly closer to the ground truth result, as is evident from the error maps.

A failure case is shown in Figure 7. In this example, apart from the high motion, the image consists of sharp features which is preserved by our network which is not detected as noise.

V. CONCLUSIONS

We propose a deep-burst denoising model based on optical flow guided alignment and cooperative filtering. A well-established single image denoising module generates pre-denoised burst input images for two different assumed noise levels. Alignment to the reference frame is performed using a state of the art optical flow network. Providing the original input burst and the pre-denoised stacks ensures the good performance of the optical flow alignment. Based on the aligned features and images a set of content-adaptive spatially-varying filter kernel is predicted to smooth each input image individually. A fusion block finally combines all intermediate results to the final denoised output. In the future, one can also compare the effect of state of the art optical flow based correspondence alignment on the quality of the burst image denosing.

Our approach yields state-of-the-art results across low noise levels on the standard benchmark data sets. Higher noise scenarios working on different pre-denoised images shows a comparable benefit.

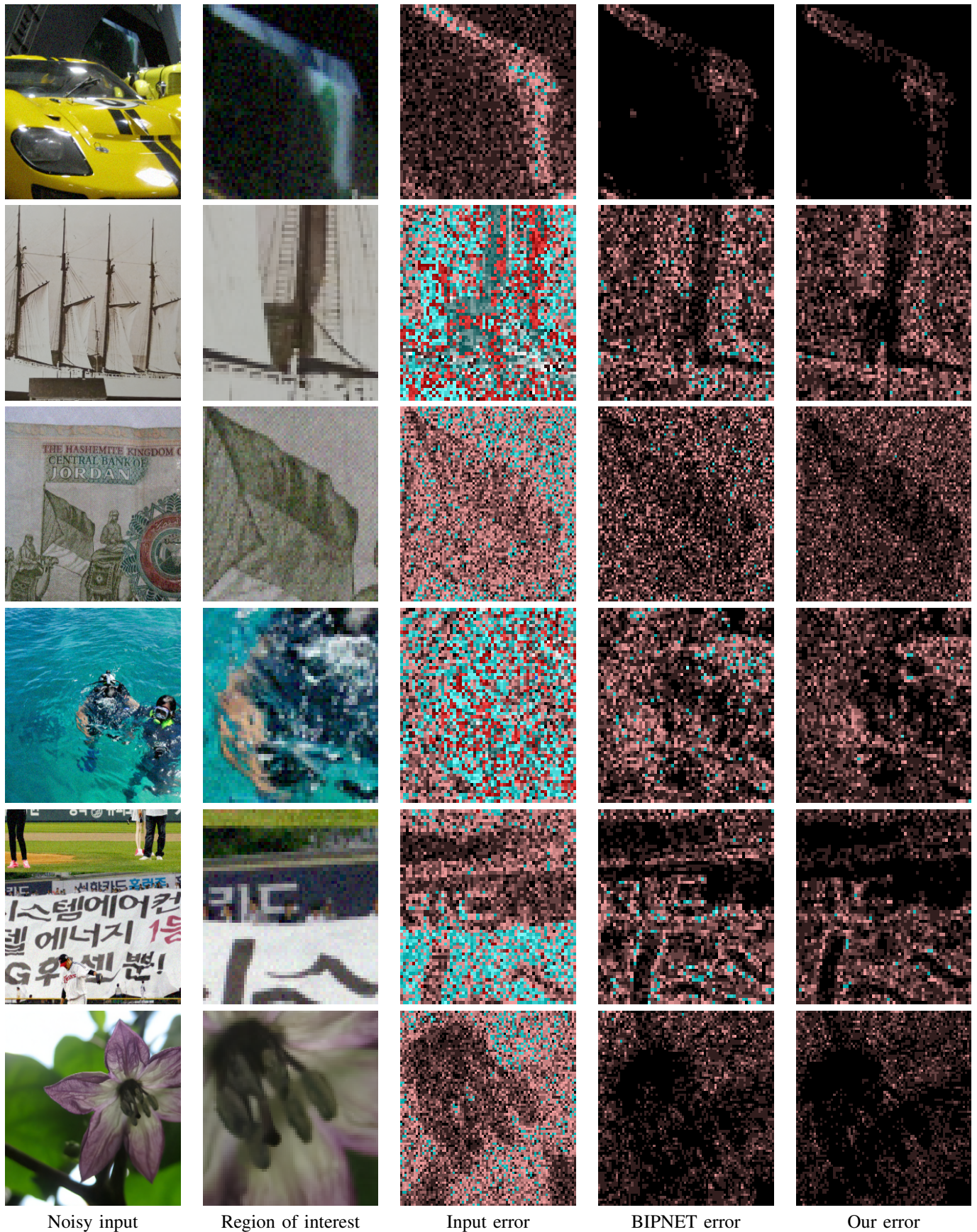
ACKNOWLEDGEMENT

This work has been partially funded by the Deutsche Forschungsgemeinschaft (DFG, German Research Foundation) under Germany's Excellence Strategy - EXC number 2064/1 - project number 390727645 and SFB 1233 - project number 276693517. It was supported by the German Federal Ministry of Education and Research (BMBF): Tübingen AI Center, FKZ: 01IS18039A and Cyber Valley. The authors thank the International Max Planck Research School for Intelligent Systems (IMPRS-IS) for supporting Arijit Mallick.

REFERENCES

- [1] A. B. Molini, D. Valsesia, G. Fracastoro, and E. Magli, "DeepSUM: Deep neural network for super-resolution of unregistered multitemporal images," *IEEE Transactions on Geoscience and Remote Sensing*, vol. 58, no. 5, pp. 3644–3656, may 2020. [Online]. Available: <https://doi.org/10.1109/2Ftgrs.2019.2959248>
- [2] M. Kawulok, P. Benecki, S. Piechaczek, K. Hrynczenko, D. Kostrzewa, and J. Nalepa, "Deep learning for multiple-image super-resolution," *IEEE Geoscience and Remote Sensing Letters*, vol. 17, no. 6, pp. 1062–1066, jun 2020. [Online]. Available: <https://doi.org/10.1109/2Ftgrs.2019.2940483>
- [3] O. Liba, K. Murthy, Y.-T. Tsai, T. Brooks, T. Xue, N. Karnad, Q. He, J. T. Barron, D. Sharlet, R. Geiss, S. W. Hasinoff, Y. Pritch, and M. Levoy, "Handheld mobile photography in very low light," *ACM*

- Transactions on Graphics*, vol. 38, no. 6, pp. 1–16, dec 2019. [Online]. Available: <https://doi.org/10.1145/2F3355089.3356508>
- [4] S. W. Hasinoff, D. Sharlet, R. Geiss, A. Adams, J. T. Barron, F. Kainz, J. Chen, and M. Levoy, "Burst photography for high dynamic range and low-light imaging on mobile cameras," *ACM Trans. Graph.*, vol. 35, no. 6, nov 2016. [Online]. Available: <https://doi.org/10.1145/2980179.2980254>
- [5] G. Bhat, M. Danelljan, L. Van Gool, and R. Timofte, "Deep burst super-resolution," 2021. [Online]. Available: <https://arxiv.org/abs/2101.10997>
- [6] B. Wronski, I. Garcia-Dorado, M. Ernst, D. Kelly, M. Krainin, C.-K. Liang, M. Levoy, and P. Milanfar, "Handheld multi-frame super-resolution," *ACM Trans. Graph.*, vol. 38, no. 4, jul 2019. [Online]. Available: <https://doi.org/10.1145/3306346.3323024>
- [7] D. Valsesia and E. Magli, "Permutation invariance and uncertainty in multitemporal image super-resolution," *IEEE Transactions on Geoscience and Remote Sensing*, vol. 60, pp. 1–12, 2022.
- [8] M. Deudon, A. Kalaitzis, I. Goytom, M. R. Arefin, Z. Lin, K. Sankaran, V. Michalski, S. E. Kahou, J. Cornebise, and Y. Bengio, "Highres-net: Recursive fusion for multi-frame super-resolution of satellite imagery," 2020. [Online]. Available: <https://arxiv.org/abs/2002.06460>
- [9] C. Godard, K. Matzen, and M. Uyttendaele, "Deep burst denoising," in *Proceedings of the European Conference on Computer Vision (ECCV)*, September 2018.
- [10] G. Bhat, M. Danelljan, F. Yu, L. V. Gool, and R. Timofte, "Deep reparametrization of multi-frame super-resolution and denoising," 2021.
- [11] S. Gu, Y. Li, L. V. Gool, and R. Timofte, "Self-guided network for fast image denoising," in *Proceedings of the IEEE/CVF International Conference on Computer Vision*, 2019, pp. 2511–2520.
- [12] Z. Teed and J. Deng, "Raft: Recurrent all-pairs field transforms for optical flow," in *European conference on computer vision*. Springer, 2020, pp. 402–419.
- [13] K. Dabov, A. Foi, V. Katkovich, and K. Egiazarian, "Image denoising by sparse 3d transform-domain collaborative filtering," 2007.
- [14] J. Xie, L. Xu, and E. Chen, "Image denoising and inpainting with deep neural networks," in *Proceedings of the 25th International Conference on Neural Information Processing Systems - Volume 1*, ser. NIPS'12. Red Hook, NY, USA: Curran Associates Inc., 2012, p. 341–349.
- [15] M. Aharon, M. Elad, and A. Bruckstein, "K-svd: An algorithm for designing overcomplete dictionaries for sparse representation," *IEEE Transactions on Signal Processing*, vol. 54, no. 11, pp. 4311–4322, 2006.
- [16] U. Schmidt and S. Roth, "Shrinkage fields for effective image restoration," in *2014 IEEE Conference on Computer Vision and Pattern Recognition*, 2014, pp. 2774–2781.
- [17] K. Zhang, W. Zuo, Y. Chen, D. Meng, and L. Zhang, "Beyond a gaussian denoiser: Residual learning of deep CNN for image denoising," *IEEE Transactions on Image Processing*, vol. 26, no. 7, pp. 3142–3155, jul 2017. [Online]. Available: <https://doi.org/10.1109/2Ftsp.2017.2662206>
- [18] X.-J. Mao, C. Shen, and Y.-B. Yang, "Image restoration using very deep convolutional encoder-decoder networks with symmetric skip connections," 2016. [Online]. Available: <https://arxiv.org/abs/1603.09056>
- [19] Y. Tai, J. Yang, X. Liu, and C. Xu, "Memnet: A persistent memory network for image restoration," 2017. [Online]. Available: <https://arxiv.org/abs/1708.02209>
- [20] H. Chen, Y. Wang, T. Guo, C. Xu, Y. Deng, Z. Liu, S. Ma, C. Xu, C. Xu, and W. Gao, "Pre-trained image processing transformer," 2020. [Online]. Available: <https://arxiv.org/abs/2012.00364>
- [21] P. Wieschollek, M. Hirsch, B. Scholkopf, and H. P. A. Lensch, "Learning blind motion deblurring," in *Proceedings of the IEEE International Conference on Computer Vision (ICCV)*, Oct 2017.
- [22] B. Mildenhall, J. T. Barron, J. Chen, D. Sharlet, R. Ng, and R. Carroll, "Burst denoising with kernel prediction networks," in *IEEE Conference on Computer Vision and Pattern Recognition (CVPR)*, 2018.
- [23] W. Cho, S. Son, and D.-S. Kim, "Weighted multi-kernel prediction network for burst image super-resolution," in *2021 IEEE/CVF Conference on Computer Vision and Pattern Recognition Workshops (CVPRW)*, 2021, pp. 404–413.
- [24] A. Dudhane, S. W. Zamir, S. Khan, F. S. Khan, and M.-H. Yang, "Burst image restoration and enhancement," in *2022 IEEE/CVF Conference on Computer Vision and Pattern Recognition (CVPR)*, 2022, pp. 5749–5758.
- [25] M. Tico, "Multi-frame image denoising and stabilization," in *2008 16th European Signal Processing Conference*, 2008, pp. 1–4.
- [26] M. Maggioni, G. Boracchi, A. Foi, and K. Egiazarian, "Video denoising, deblurring, and enhancement through separable 4-d nonlocal spatiotemporal transforms," *IEEE Transactions on Image Processing*, vol. 21, no. 9, pp. 3952–3966, 2012.



Noisy input

Region of interest

Input error

BIPNET error

Our error

Figure 6. Qualitative performance of our algorithm with respect to BIPNET [24] on the evaluation color dataset. Notice the excessive smoothing by BIPNET which removes the sharper features in comparison to the ground truth. Our network retains the details and removes the noise as well. Darker region corresponds to lesser error which indicates better denoising. It is to be noted that the error maps have been scaled 5 times for better visual understanding.

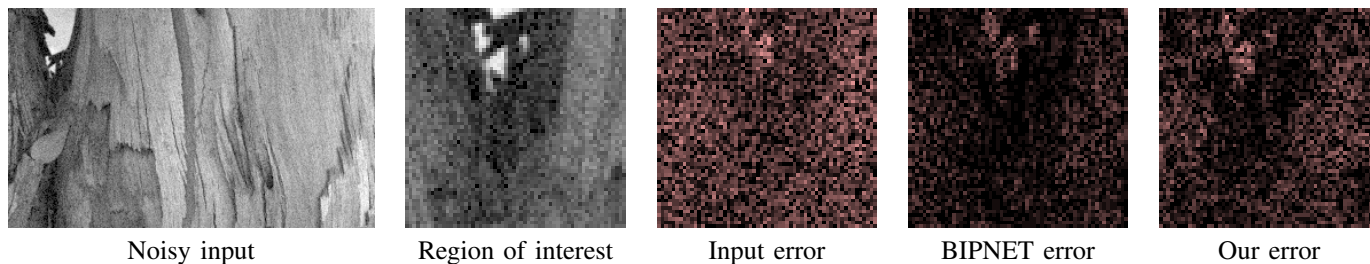


Figure 7. Worst performing images in the test set. The excessive noise in the input combined with strong camera motion deteriorates the denoising performance. It is to be noted that the error maps have been scaled 2 times for better visual understanding.

- [27] K. Dabov, A. Foi, and K. Egiazarian, "Video denoising by sparse 3d transform-domain collaborative filtering," in *2007 15th European Signal Processing Conference, 2007*, pp. 145–149.
- [28] A. Bruhn, J. Weickert, and C. Schnörr, "Lucas/kanade meets horn/schunck: Combining local and global optic flow methods," *International journal of computer vision*, vol. 61, no. 3, pp. 211–231, 2005.
- [29] A. Buades, J.-L. Lisani, and M. Miladinović, "Patch-based video denoising with optical flow estimation," *IEEE Transactions on Image Processing*, vol. 25, no. 6, pp. 2573–2586, 2016.
- [30] A. Dosovitskiy, P. Fischer, E. Ilg, P. Hausser, C. Hazirbas, V. Golkov, P. Van Der Smagt, D. Cremers, and T. Brox, "FlowNet: Learning optical flow with convolutional networks," in *Proceedings of the IEEE international conference on computer vision*, 2015, pp. 2758–2766.
- [31] E. Ilg, N. Mayer, T. Saikia, M. Keuper, A. Dosovitskiy, and T. Brox, "FlowNet 2.0: Evolution of optical flow estimation with deep networks," in *Proceedings of the IEEE conference on computer vision and pattern recognition*, 2017, pp. 2462–2470.
- [32] Z. Huang, X. Shi, C. Zhang, Q. Wang, K. C. Cheung, H. Qin, J. Dai, and H. Li, "Flowformer: A transformer architecture for optical flow," *arXiv preprint arXiv:2203.16194*, 2022.
- [33] D. J. Butler, J. Wulff, G. B. Stanley, and M. J. Black, "A naturalistic open source movie for optical flow evaluation," in *European Conf. on Computer Vision (ECCV)*, ser. Part IV, LNCS 7577, A. Fitzgibbon et al. (Eds.), Ed. Springer-Verlag, Oct. 2012, pp. 611–625.
- [34] A. Paszke, S. Gross, F. Massa, A. Lerer, J. Bradbury, G. Chanan, T. Killeen, Z. Lin, N. Gimelshein, L. Antiga, A. Desmaison, A. Kopf, E. Yang, Z. DeVito, M. Raison, A. Tejani, S. Chilamkurthy, B. Steiner, L. Fang, J. Bai, and S. Chintala, "Pytorch: An imperative style, high-performance deep learning library," in *Advances in Neural Information Processing Systems 32*, H. Wallach, H. Larochelle, A. Beygelzimer, F. d'Alché-Buc, E. Fox, and R. Garnett, Eds. Curran Associates, Inc., 2019, pp. 8024–8035. [Online]. Available: <http://papers.neurips.cc/paper/9015-pytorch-an-imperative-style-high-performance-deep-learning-library.pdf>
- [35] D. P. Kingma and J. Ba, "Adam: A method for stochastic optimization," *arXiv preprint arXiv:1412.6980*, 2014.
- [36] Y. ZHAO, "PyTorch implementation of Self Guided Network (ICCV)," 2019. [Online]. Available: <https://github.com/zhaoyuzhi/Self-Guided-Network-for-Fast-Image-Denoising>
- [37] I. Krasin, T. Duerig, N. Alldrin, V. Ferrari, S. Abu-El-Haija, A. Kuznetsova, H. Rom, J. Uijlings, S. Popov, S. Kamali, M. Mallocci, J. Pont-Tuset, A. Veit, S. Belongie, V. Gomes, A. Gupta, C. Sun, G. Chechik, D. Cai, Z. Feng, D. Narayanan, and K. Murphy, "Openimages: A public dataset for large-scale multi-label and multi-class image classification." *Dataset available from <https://storage.googleapis.com/openimages/web/index.html>*, 2017.
- [38] G. Healey and R. Kondepudy, "Radiometric ccd camera calibration and noise estimation," *IEEE Transactions on Pattern Analysis and Machine Intelligence*, vol. 16, no. 3, pp. 267–276, 1994.
- [39] Z. Xia, F. Perazzi, M. Gharbi, K. Sunkavalli, and A. Chakrabarti, "Basis prediction networks for effective burst denoising with large kernels," in *2020 IEEE/CVF Conference on Computer Vision and Pattern Recognition (CVPR)*, 2020, pp. 11 841–11 850.